Harnessing competitive interactions to regulate supramolecular "micelle-droplet-fiber" transition and reversibility in water

Heleen Duijs,[a] Shikha Dhiman,*[b] and Lu Su*[a]

[a]Division of Biotherapeutics, Leiden Academic Centre for Drug Research (LACDR), Leiden University, Einsteinweg 55, 2333 CC Leiden, The Netherlands.

[b] Department of Chemistry, Johannes Gutenberg University in Mainz, Duesbergweg 10-14, D-55128 Mainz, Germany.

ABSTRACT: Supramolecular assembly of proteins into irreversible fibrils is often associated with diseases where aberrant phase transitions occur. Due to the complexity of biological systems and their surrounding environments, the mechanism underlying phase separation-mediated supramolecular assembly is poorly understood, making the reversal of so-called irreversible fibrillization a significant challenge. Therefore, it is crucial to develop simple model systems that provide insights into the mechanistic process of monomers to phase-separated droplets to ordered supramolecular assemblies. Such models can help in investigating strategies to either reverse or modulate these states. Herein, we present a simple synthetic model system composed of three components, including a benzene-1,3,5-tricarboxamide-based supramolecular monomer, a surfactant, and water, to mimic the condensate pathway observed in biological systems. This highly dynamic system can undergo "micelle-droplet-fiber" transition over time and space with a gradient field, regulated by competitive interactions. Importantly, manipulating these competitive interactions through guest molecules, temperature changes, and co-solvent can reverse the ordered fibers back into a disordered liquid or micellar state. Our model system provides new insights into the critical balance between various interactions among the three components that determine the pathway and reversibility of the process. Extending this 'competitive-interactions' approach from a simple model system to complex macromolecules, e.g., proteins, could open new avenues for biomedical applications, such as condensate-modifying therapeutics.

INTRODUCTION

Supramolecular assembly is fundamental to the formation of many complex biological structures, for instance, protein filaments, DNA, and membranes.[1] Its non-covalent nature enables dynamic assemblies of divergent building blocks, allowing for drastic conformational or functional changes in response to slight alterations in chemical environment.[2–5] Competitive interactions are critical in modulating the chemical environment, thereby influencing the supramolecular energy landscape and the resulting order in the structures.[6] Among these, the supramolecular assembly of proteins into fibrils can be mediated by the process of liquid-liquid phase separation (LLPS).[7,8] This process clusters monomers into solute-rich droplets, thereby facilitating nucleation and promoting the fiber formation.[9] This LLPS-mediated fiber growth is displayed by natural building blocks, such as intrinsically disordered proteins or peptides.[8,10–14] Recently, it has been observed that even small synthetic molecules can form liquid droplets, either at equilibrium or at metastable state *enroute* to supramolecular polymerization.[15,16] This suggests a general mechanism of LLPS-mediated supramolecular polymerization, proving the versatility of synthetic supramolecular building blocks as mimics of natural systems.[17] This emphasizes the role of phase separation in driving supramolecular polymerization, which is yet to be completely understood.

In the biological realm, the aberrant transition from liquid droplets into ordered solid protein aggregates is increasingly associated to the onset and progression of diseases.[18–25] Novel mechanistic insights are gradually being uncovered. For example, RNA concentration affects phase separation-mediated fibrilization of RNA-binding proteins, demonstrating that competitive interactions can regulate the condensation pathway.[26] However, the study of reversing protein aggregation remains elusive.[27] Understanding phase separation-mediated fibrilization should therefore be expanded into a general concept using a simple supramolecular model system. This model system will allow exploration of strategies to intervene with the solid aggregates and return to the liquid state, aiming to develop effective treatments for protein condensate-related diseases.[28]

We hypothesize that it is possible to regulate the supramolecular pathway between liquid droplets and fibril state through competitive interactions due to their non-covalent nature. To explore this hypothesis, we propose a model system composed of highly dynamic small molecules that can be easily manipulated and studied through microscopy and spectroscopy. We selected the highly dynamic benzene-1,3,5-tricarboxamide motif, functionalized with amphiphilic tails composed of dodecyl and tetraethylene glycol (BTA-EG_4, BTA in short hereafter, Figure 1), as it forms one-dimensional fibers driven by π-π stacking and hydrogen bonds, and is capable of reorganizing in response to stimuli in water.[29–34] We serendipitously observed that introducing the surfactant cetrimonium bromide (CTAB) into BTA supramolecular polymers can break down the long fibers and lead to complete disassembly at optimized ratio and

concentration. Interestingly, the supramolecular polymerization is reinstated through an intermediate liquid droplet state upon dilution. [35] We hypothesize that this reversibility originates from the competitive interactions among the three components: BTA, surfactant, and water. Therefore, in this study, we demonstrate the role of competitive interactions in regulating condensate dynamics and fibril formation with the BTA-surfactant model system in water (Figure 1).

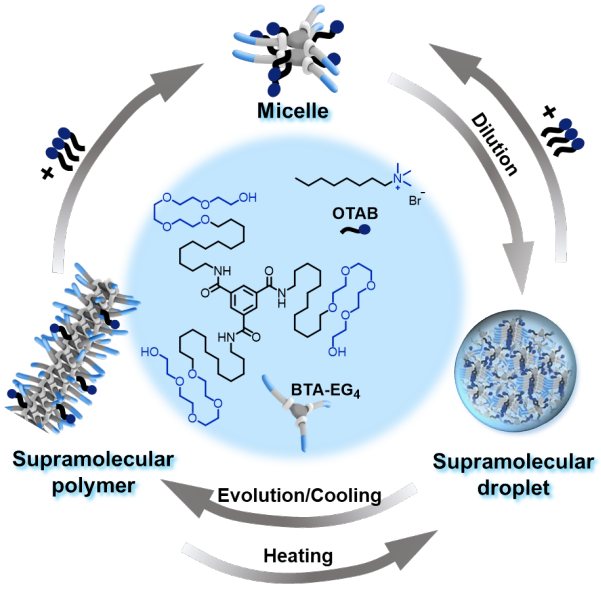

Figure 1. Schematic illustration of supramolecular "micelle-droplet-fiber" transition of BTA-OTAB system upon regulation of the competitive interactions.

RESULTS AND DISCUSSION

Rational design. To explore the energy landscape of BTA-surfactant system, we used octyltrimethylammonium bromide (OTAB) as the surfactant. Due to the shorter alkyl chain length of OTAB compared to CTAB, it exhibits weaker hydrophobic interactions with BTA. This allows us to slow down the dynamics of the system at millimolar (mM) concentration regimes, thereby expanding the operational window and fine-tuning the transitions. This tunability is critical for exploring the mechanistic aspects of supramolecular phase transition and its regulation by competitive interactions. BTA and Cyanine 5 labeled BTA (BTA-Cy5, Figure S1) for fluorescence imaging were synthesized and characterized following previous reports.[29,36]

Supramolecular "micelle-droplet-fiber" transition using a concentration gradient field. To create a concentration gradient of BTA-OTAB, we use a dual-inlet channel by introducing [BTA]:[OTAB] solution (31:202 mM with 25 μM BTA-Cy5, *sample preparation method II*) and milli-Q (MQ) water from the two inlets separately (Figure 2A). We investigated the effect of this concentration gradient with confocal laser scanning microscopy (CLSM). Initially, the BTA-OTAB is a homogenous micellar solution with the C_8 aliphatic chain of OTAB inserted into BTA hydrophobic pockets. Dilution of the micellar phase weakens BTA-OTAB interactions, resulting in the partial release of OTAB from BTA-OTAB micelles and promoting LLPS. At the interface of the two solutions, supramolecular droplets were observed (Figure 2A, Figure S2). Interestingly, these droplets appeared in both spherical and non-spherical shapes, which can be explained by the polymer phase diagram as predicted by Flory-Huggins theory (Figure S3).[37–40] These droplets can coalesce (Figure 2B), confirming their liquid properties. Near the water inlet, micrometer-long fibers were present (Figure S2) as a result of the stacking of the newly exposed BTA. We identified five different stages within BTA-OTAB system: micelles (I), inverse droplets (II), non-spherical droplets (III), droplets (IV) and fibers (V) (Figure 2A, Figure S3). The spherical droplets (II and IV) emerge from nucleation and growth, while the non-spherical droplets (III) either emerge from spinodal decomposition[41] or from growth of inverse droplets (II).[42] Cryogenic transmission electron microscopy (cryo-TEM, *Sample preparation method VI*) showed a similar phase transition pattern with a mixture of spherical droplets, non-spherical droplets, and fibers at the interface layer (Figure 2E, Figure S4), and densely packed fibers at the water layer (Figure S5).

Fluorescence recovery after photobleaching (FRAP) was performed at different stages to evaluate the dynamics of BTA-OTAB supramolecular structures (Figure 2C). All fluorescent signals recovered within approximately 2 min, which is faster in comparison to the recovery of BTA fibers alone (15% recovery in 4 min, Figure S6), indicating that OTAB significantly interferes with and weakens the BTA-BTA interactions. The apparent diffusion coefficients (D_{FRAP}) of each state, derived from the fitted recovery curves, showed a consistent decrease from $6.5 \cdot 10^{-6}$ m^2/sec for the micelles (I), to $3.4 \cdot 10^{-6}$ m^2/sec for the inverse droplets (II), to $2.2 \cdot 10^{-6}$ m^2/sec for the non-spherical droplets (III), and eventually to $1.6 \cdot 10^{-6}$ m^2/sec for the droplets (IV) (Figure 2D), indicating a slowdown in dynamics. This trend can be attributed to an increase in inter-monomer and/or inter-oligomer interactions, driven by the gradual release of the OTAB and greater exposure of BTA hydrophobic pockets. Fibers (V) are expected to have an even slower diffusion, yet a relatively fast recovery with a D_{FRAP} of $2.8 \cdot 10^{-6}$ m^2/sec was observed, probably due to the presence of OTAB in the BTA fiber networks (Figure S6).

As control experiments, replacing MQ water with a 16 or 31 mM OTAB solution resulted in transient phase separation, while higher OTAB concentrations (47, 101 or 202 mM) showed neither phase separation nor fibers, but only a homogenous micellar solution (Figures S7, S8). This suggests that competitive interactions among the three components—BTA, surfactant, and water—modulate the order of the system through "micelle-droplet-fiber" transition. Therefore, in the following study, we investigate the molecular interaction in more detail.

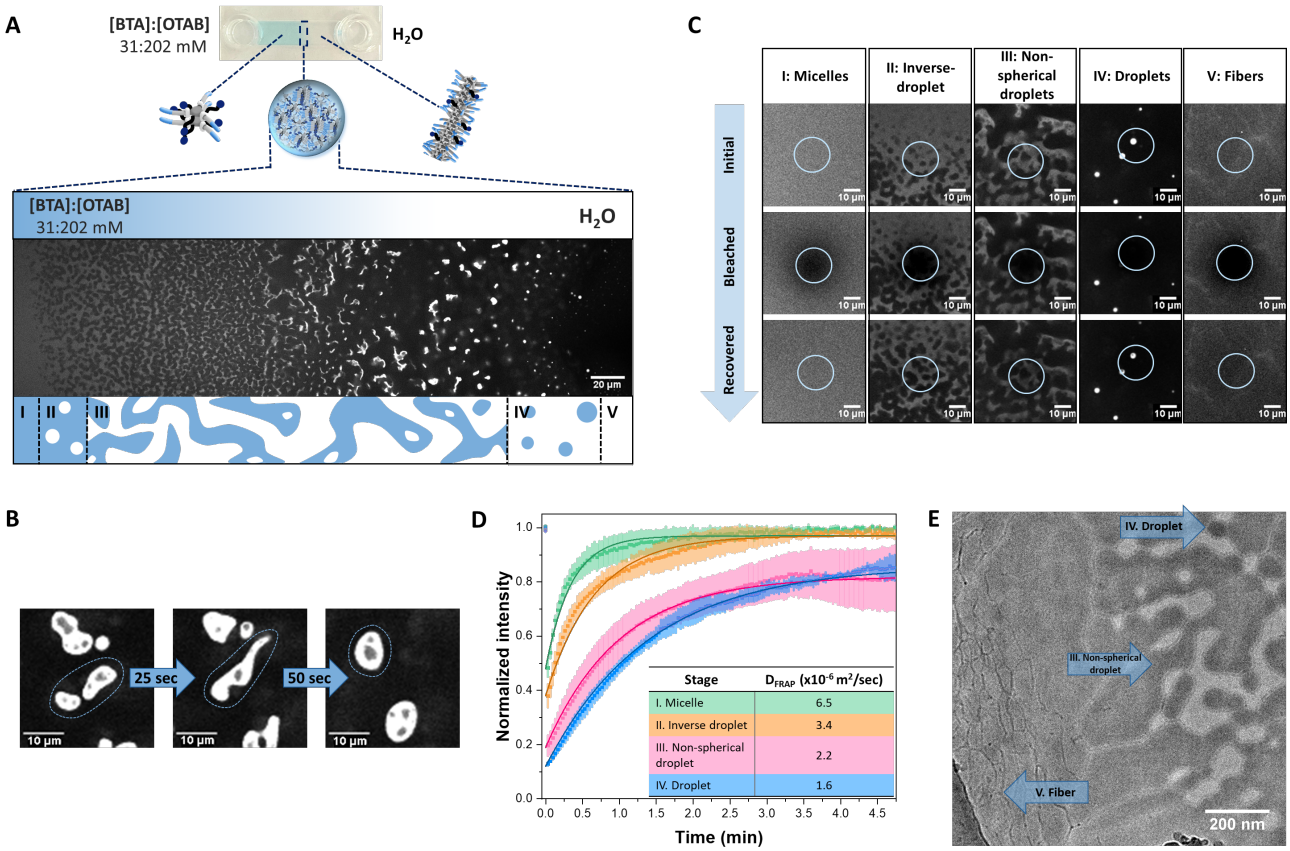

Figure 2. Supramolecular "micelle-droplet-fiber" transition using a concentration gradient field in BTA-OTAB system. (A) CLSM image through a dual-inlet channel of a concentration gradient from [BTA]:[OTAB] (31:202 mM with 25 μM BTA-Cy5) to MQ water which induces supramolecular "micelle-droplet-fiber" transition at the interface, scale bar = 20 μm. Below, a schematic overview is given to compare the shape of the droplets with the processes of nucleation & growth ,and spinodal decomposition. (B) CLSM images of droplet coalescence over time, indicated with a dashed circle, scale bar = 10 μm. (C) CLSM images of the various supramolecular structures before and after fluorescent bleaching at different stages (I-V) of BTA-OTAB system, scale bar = 10 μm. (D) Exponential fitting of FRAP curves of stages (I-IV) with corresponding D_{FRAP}. (E) Cryo-TEM image of BTA-OTAB turbid solution (*Sample preparation method VI*), showing a phase separation pattern with a mixture of spherical droplets, non-spherical droplets, and 1D fibers, scale bar = 200 nm.

Supramolecular "micelle-droplet-fiber" transition over time upon dilution. The time evolution of BTA-OTAB morphologies upon dilution was initially observed by CLSM, where the droplets faded and converted into a fiber network within approximately 15 min at 22 °C (Figure 3A), whereas the droplets maintained their shape more than 1 h at 37 °C. At lower temperature, fiber formation is more thermodynamically favored. Whilst at higher temperature, the monomers are more dynamic, hindering supramolecular polymerization, which results in the prolonged stability of the droplets.[43] This allows us to manipulate the landscapes of the transition with temperature in the latter study. Nevertheless, capturing the droplets exclusively is challenging, as they start to convert into fibers upon mixing. We attempt to understand these intermediate states, which are probably a mixture of droplets and short fibers. To gain a deeper mechanistic insight into this "micelle-droplet-fiber" transition, we employed a combination of proton and diffusion-ordered nuclear magnetic resonance spectroscopies (^{1}H and DOSY NMR), Ultraviolet-visible (UV-Vis) and Nile red fluorescence spectroscopies, together with cryo-TEM (Figures 3, S9-S20).

For all NMR measurements, an external standard, 3-(trimethylsilyl)propionic-2,2,3,3-d_4 acid sodium salt (TPS), in a capillary NMR tube, was employed to ensure proper alignment (chemical shift = 0.0 ppm, Figures S9-12), and to serve as an indicator for the amount of portable OTAB. As depicted in Figure 3B, ^{1}H NMR spectrum of initial micellar state ([BTA]:[OTAB] = 31:202 mM, *sample preparation method I*) showed sharp and well-split peaks for both BTA (signals in blue boxes) and OTAB. Upon a two-fold dilution, the micellar solution immediately became visually turbid, indicating phase separation and the formation of droplets corresponding to stages II-IV (Figure S13). The NMR peaks corresponding to OTAB remained sharp and well-resolved. The peaks associated with BTA showed slight broadening and a decrease in integrals, with the most significant reduction from the aliphatic chain (Table S1), suggesting that the hydrophobic interactions of the C_{12}-linker initially drive phase separation. After vigorous mixing and a 24 h incubation, the BTA peaks disappeared due to the slow diffusion of the large BTA fibers, as corroborated by cryo-TEM (Figure S14). The OTAB integral dropped by approximately 10%, indicating that these 10% OTAB molecules were associated with the BTA fibers.

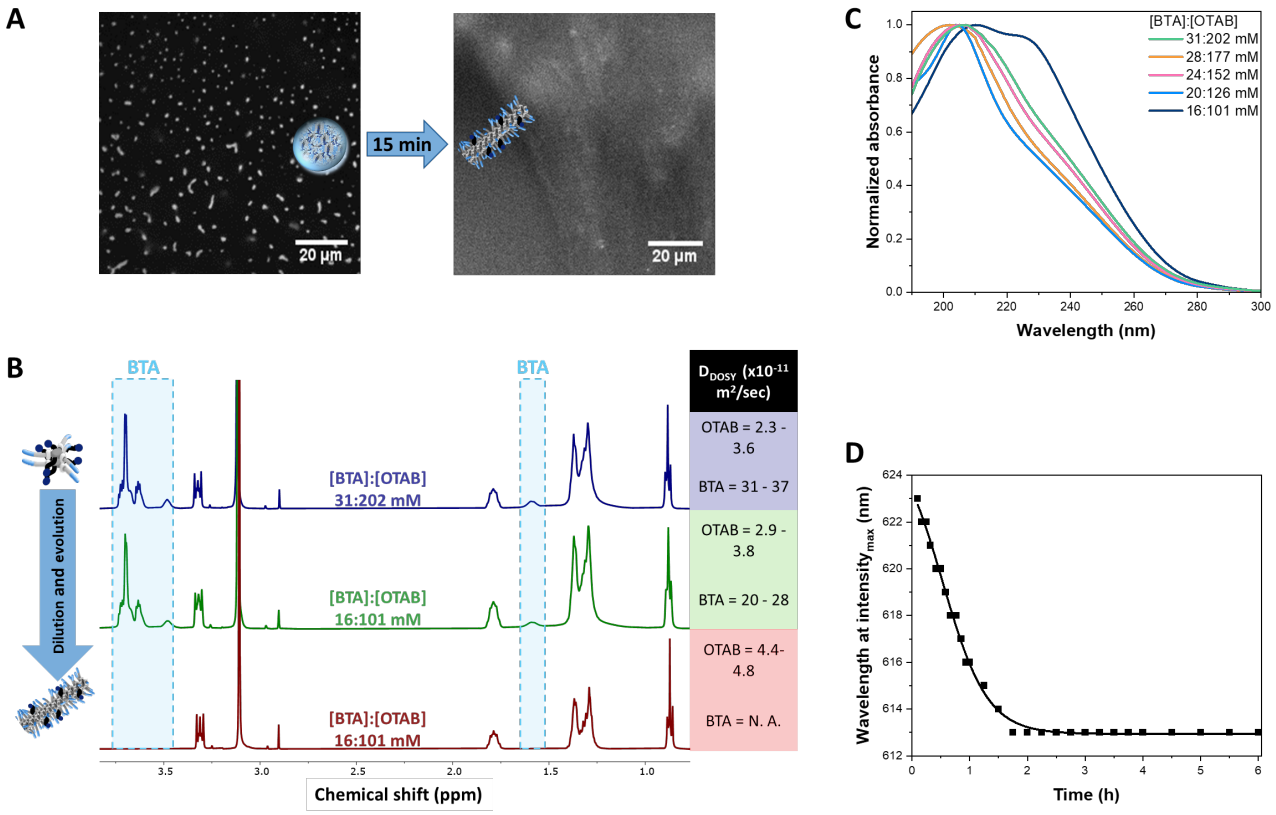

Figure 3. Temporal control of dilution-induced supramolecular transition. (A) CLSM images of the transition from supramolecular droplets into a fiber network over 15 min at 22 °C, scale bar = 20 µm. (B) Stacked ^{1}H NMR spectra of [BTA]:[OTAB] micelles (31:202 mM), supramolecular droplets (16:101 mM) and fibers (16:101 mM) in D_2O with their corresponding D_{DOSY}. (C) UV spectra of different concentrations of [BTA]:[OTAB], yet with a fixed ratio (*sample preparation method III*). The absorption of OTAB is subtracted from all measurements. (D) Time-dependent fluorescence emission of Nile red in freshly prepared [BTA]:[OTAB] (16:101 mM, *sample preparation method II*).

We subsequently assessed the translational diffusion coefficients (D_{DOSY}) of the assemblies using DOSY NMR (Figures 3B, S15-S18). Due to the fast exchange and high dynamic, two interesting phenomena were observed: i) The D_{DOSY} of BTA and OTAB were always in two distinct populations throughout the dilution and evolution processes; ii) The D_{DOSY} of both BTA and OTAB were no single values, but fell within narrow regimes. Specifically, the D_{DOSY} of OTAB increased as it transitioned from the micellar state to the supramolecular droplets and eventually to the fiber state. This faster diffusion is attributed to OTAB being gradually expelled from BTA hydrophobic pockets, which weakens the BTA-OTAB interaction. In contrast, the D_{DOSY} of BTA decreased upon dilution, reflecting the slower diffusion of the forming droplets/short fibers, driven by enhanced BTA-BTA interaction. In the final micrometer-long fiber state, the BTA signal became nondetectable.

The UV spectra at decreasing concentrations of [BTA]:[OTAB] with a constant ratio showed a red shift in the absorption, from a characteristic micellar state ([BTA]:[OTAB] = 31:202 mM) with a maximum absorption (λ_{max}) around 204 nm, to a BTA double-helix fiber state ([BTA]:[OTAB] = 16:101 mM) with maxima of 211 and 227 nm (*sample preparation method III*; Figures 3C, S19).[44] Nile red fluorescence spectroscopy further demonstrated a blue-shift of emission λ_{max} from 623 nm to 613 nm, indicating that Nile red is experiencing a more hydrophobic environment over time (*sample preparation method II;* Figure 3D, Figure S20).[16] These two techniques confirm the transition to fibers, upon dilution and its elongation over time.

Reversibility of fiber-to-droplet and droplet-to-micelle using competitive interactions. With the understanding of the competitive interactions to regulate the supramolecular "micelle-droplet-fiber" transition, we subsequently investigate different strategies based on these competitive interactions as a general concept to modulate the supramolecular landscapes of these transitions.

Reversible fiber to droplet transition. We recently observed that BTA fiber itself started depolymerizing at 60 °C, and initiated droplet formation above 80 °C, owing to the dehydration of the tetraethylene glycol.[16] Remarkably, introducing [OTAB] =101 mM in the BTA system ([BTA] = 16 mM) significantly decreases the onset temperature of depolymerization to 30 °C and fiber-to-droplet transition to 45 °C, as indicated by the scattering effect at 300 nm (*sample preparation method V*; Figures 4A, S21). This was also confirmed with CLSM that the fiber network started to convert to droplets at 40 °C, and a complete transition to droplets was displayed at 50 °C (*sample preparation method V*; Figure 4B). The decreased phase separation temperature from 80 °C to 40 °C can be attributed to the weakened BTA-

BTA interactions where OTAB disturbs the one-dimensional ordered arrangement of the BTA-core. Thereof, the fibers are broken down into short-fibers, meanwhile exposure of the hydrophobic pockets serves as a driving force for the formation of droplets. To further confirm the fiber-to-droplet transition, temperature-dependent fluorescence emission spectra were recorded with Nile red, that embedded in a mixture of BTA-OTAB fiber state (*sample preparation method V*; Figure 4C, S22). Depolymerization and droplet formation were verified by a red-shift of the emission λ_{max} from 608 to 623 nm, while λ_{max} of Nile red in water as a control showed a minor blue-shift of 2 nm (Figure S22E). Remarkably, the fiber-to-droplet transition is not unidirectional, but it can be reversed multiple times by changing the temperature by just 7 °C (*sample preparation method V*; Figure 4D). At 40 °C the fiber state dominates, while at 47 °C droplets form the major proportion. In contrast to previously reported systems, the competitive interactions encoded in the dynamic nature of the BTA-OTAB system allows for a highly responsive fiber-droplet dynamic equilibrium.

The BTA:OTAB ratio effect in the fiber-droplet transition was further investigated with variable temperature UV-Vis spectroscopy. While [BTA] was fixed at 16 mM, [OTAB] was gradually increased beyond 101 mM. The onset temperature of depolymerization decreased from approximately 35 °C to 25 °C (*sample preparation method IV*; Figure 4E), while the phase transition temperature increased from 50 °C to 60 °C for [OTAB] from 101 to 124 mM (*sample preparation method IV*; Figures 4F, S24). We hypothesize that above a critical OTAB ratio, the hydrophobic BTA-BTA interactions are completely overcome by addition of cationic charge of OTAB. This repulsive interaction decreases the depolymerization energy barrier. In addition, the droplets state is majorly driven by the dehydration of tetraethylene glycol, resulting in a higher onset temperature of phase separation.

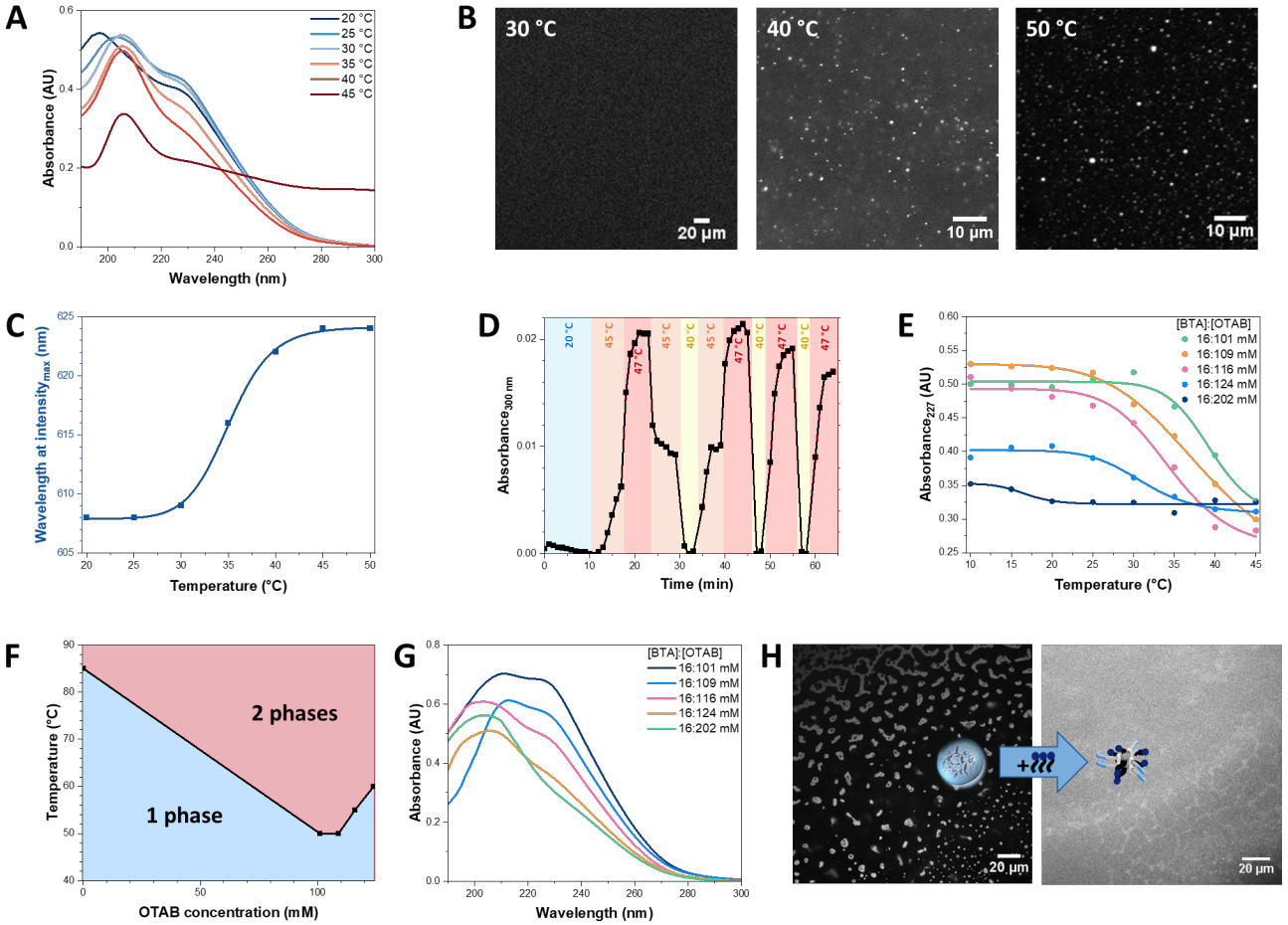

Figure 4. Reversibility of fibers and droplets by tuning of competitive interactions. (A) Temperature-dependent UV spectrum of [BTA]:[OTAB] 16:101 mM (*sample preparation method V)*; (B) Temperature-dependent CLSM images at of [BTA]:[OTAB] 16:101 mM with 25 µM BTA-Cy5 (*sample preparation method V)*; (C) Temperature-dependent fluorescence emission of [BTA]:[OTAB] 16:101 mM with 20 µM Nile red (*sample preparation method V)*; (D) Absorbance at 300 nm during temperature cycles of [BTA]:[OTAB] 16:101 mM with 20 µM Nile red (*sample preparation method V)*; (E) Absorbance at 227 nm of several [BTA]:[OTAB] ratios by varying the temperature from 20 to 45 °C (*sample preparation method IV)*; (F) Phase separating temperature at several [BTA]:[OTAB] ratios (*sample preparation method IV)*; (G) UV spectrum of [BTA]:[OTAB] with varying OTAB concentration (*sample preparation method IV)*; (H) CLSM images of BTA-OTAB droplets in a concentration gradient by a dual-inlet chamber system, before and after addition of 202 mM OTAB, Scale bar = 20 µm. Absorption of OTAB is subtracted from all UV measurements.

Reversible droplets to micelles transition. At [BTA]:[OTAB] = 16:202 mM, a complete micellar state was reached, thereof no depolymerization or phase separation was detected even up to 80 °C (s*ample preparation method IV*; Figures 4G, S23, S24E). This is depicted by the UV spectra showing a characteristic micellar absorption at 204 nm. Interestingly, the micelle-to-droplet transition is reversible by introducing additional OTAB. This is observed in CLSM images, where supramolecular droplets at the interface of [BTA]:[OTAB] (31:202 mM) to H_2O in the dual-inlet chamber system converted to a homogenous micellar solution upon addition OTAB solution in the water phase (s*ample preparation method II*; Figure 4H).

To generalize the role of competitive interactions in determining the supramolecular state., we evaluated solvent polarity using a methanol-water mixture. [BTA]:[OTAB] (31:202 mM) and 5% or 8% methanol in water were injected in either inlet of the channel (Figure S25). It was observed that supramolecular droplet or fiber formation can be inhibited by competitive interaction of 8% methanol. At 5% methanol still some traces of supramolecular droplets were observed at the interface of the two solutions.

CONCLUSION

In this study, we demonstrate the role of competitive interactions in determining the supramolecular landscape and the extent of order in the system. Due to the dynamic and non-covalent nature of BTA assemblies, the concentration of competitive guest and temperature regulate the micelle, droplet or polymer state, as well as their transition points. Through this model system, we reiterate that balances between various interactions are crucial. At molecular level, these are interactions between monomer, guest and solvent, not only at the monomer core, but also at the tails. At supramolecular level, these are the intermonomer and inter-fiber interactions that influence the pathway of assembly and disassembly. However, expanding this understanding from simple synthetic molecules with limited possibilities of intermolecular interactions to complex macromolecules such as proteins requires comprehensive studies using combined experimental and theoretical approaches. This would provide us with a large database that can use artificial intelligence to predict the required competing guests or key interprotein interactions that need to be targeted. These key interprotein interactions need special attention for mechanistic understanding and drug designing for condensate-modifying therapeutics. [45,46]

ASSOCIATED CONTENT

Supporting Information.
Experimental details; supporting figures of fluorescent microscopy, NMR characterization, spectroscopic characterization, cryoTEM images, and CLSM videos of coalescence or deformation. This material is available free of charge via the Internet at http://pubs.acs.org.

AUTHOR INFORMATION

Corresponding Author

Lu Su - orcid.org/0000-0001-8207-756X; Email: l.su@lacdr.leidenuniv.nl.

Shikha Dhiman - orcid.org/0000-0001-9180-507; Email: shikha.dhiman@uni-mainz.de.

Authors

Heleen Duijs: orcid.org/0009-0003-0544-513X

Author Contributions

The manuscript was written through contributions of all authors. All authors have given approval to the final version of the manuscript.

Funding Sources

L.S. acknowledges starter grant from The Dutch Research Council (NWO).

Notes

The authors declare that the research was conducted in the absence of any commercial or financial relationships that could be construed as a potential conflict of interest.

ACKNOWLEDGMENT

We thank Prof. E. W. Meijer for the valuable discussions, continuous support and for providing BTA and BTA-Cy5. We acknowledge the ICMS Animation Studio for support with the artwork. H.D. and L.S. thank Prof. Matthias Barz for the discussions, Dr. Karthick Sai Sankar Gupta for support during NMR characterization, Mr. Kostas Tassis for support for CLSM imaging, and Dr. Willem Noteborn in NeCEN for support during Cryo-TEM measurements.

REFERENCES

(1) Mattia, E.; Otto, S. Supramolecular Systems Chemistry. Nat Nanotechnol 2015, 10 (2), 111–119. https://doi.org/10.1038/nnano.2014.337.

(2) Lenne, P. F.; Trivedi, V. Sculpting Tissues by Phase Transitions. Nat Commun 2022, 13 (1), 1–14. https://doi.org/10.1038/s41467-022-28151-9.

(3) McManus, J. J.; Charbonneau, P.; Zaccarelli, E.; Asherie, N. The Physics of Protein Self-Assembly. Curr Opin Colloid Interface Sci 2016, 22, 73–79. https://doi.org/10.1016/j.cocis.2016.02.011.

(4) Wang, C.; Fu, L.; Hu, Z.; Zhong, Y. A Mini-Review on Peptide-Based Self-Assemblies and Their Biological Applications. Nanotechnology 2022, 33 (6), 062004. https://doi.org/10.1088/1361-6528/ac2fe3.

(5) Jacobs, W. M.; Frenkel, D. Phase Transitions in Biological Systems with Many Components. Biophys J 2017, 112 (4), 683–691. https://doi.org/10.1016/j.bpj.2016.10.043.

(6) Mattia, E.; Otto, S. Supramolecular Systems Chemistry. Nat Nanotechnol 2015, 10 (2), 111–119. https://doi.org/10.1038/nnano.2014.337.

(7) Yuan, C.; Levin, A.; Chen, W.; Xing, R.; Zou, Q.; Herling, T. W.; Challa, P. K.; Knowles, T. P. J.; Yan, X. Nucleation and Growth of Amino Acid and Peptide Supramolecular Polymers through Liquid–Liquid Phase Separation. Angewandte Chemie International Edition 2019, 58 (50), 18116–18123. https://doi.org/10.1002/anie.201911782.

(8) Yuan, C.; Li, Q.; Xing, R.; Li, J.; Yan, X. Peptide Self-Assembly through Liquid-Liquid Phase Separation. Chem 2023, 9 (9), 2425–2445. https://doi.org/10.1016/j.chempr.2023.05.009.

(9) Chang, R.; Yuan, C.; Zhou, P.; Xing, R.; Yan, X. Peptide Self-Assembly: From Ordered to Disordered. Acc Chem Res 2024, 57 (3), 289–301. https://doi.org/10.1021/acs.accounts.3c00592.

(10) Lin, Y.; Fichou, Y.; Longhini, A. P.; Llanes, L. C.; Yin, P.; Bazan, G. C.; Kosik, K. S.; Han, S. Liquid-Liquid Phase Separation of Tau Driven by Hydrophobic Interaction Facilitates Fibrillization of Tau.

J Mol Biol 2021, 433 (2), 166731. https://doi.org/10.1016/j.jmb.2020.166731.
(11) Reber, S.; Jutzi, D.; Lindsay, H.; Devoy, A.; Mechtersheimer, J.; Levone, B. R.; Domanski, M.; Bentmann, E.; Dormann, D.; Mühlemann, O.; Barabino, S. M. L.; Ruepp, M. D. The Phase Separation-Dependent FUS Interactome Reveals Nuclear and Cytoplasmic Function of Liquid-Liquid Phase Separation. Nucleic Acids Res 2021, 49 (13), 7713–7731. https://doi.org/10.1093/nar/gkab582.
(12) Leppert, A.; Chen, G.; Lama, D.; Sahin, C.; Railaite, V.; Shilkova, O.; Arndt, T.; Marklund, E. G.; Lane, D. P.; Rising, A.; Landreh, M. Liquid–Liquid Phase Separation Primes Spider Silk Proteins for Fiber Formation via a Conditional Sticker Domain. Nano Lett 2023, 23 (12), 5836–5841. https://doi.org/10.1021/acs.nanolett.3c00773.
(13) Zhou, P.; Xing, R.; Li, Q.; Li, J.; Yuan, C.; Yan, X. Steering Phase-Separated Droplets to Control Fibrillar Network Evolution of Supramolecular Peptide Hydrogels. Matter 2023, 6 (6), 1945–1963. https://doi.org/10.1016/j.matt.2023.03.029.
(14) Yoshizawa, T.; Nozawa, R. S.; Jia, T. Z.; Saio, T.; Mori, E. Biological Phase Separation: Cell Biology Meets Biophysics. Biophys Rev 2020, 12 (2), 519–539. https://doi.org/10.1007/s12551-020-00680-x.
(15) Fu, H.; Huang, J.; van der Tol, J. J. B.; Su, L.; Wang, Y.; Dey, S.; Zijlstra, P.; Fytas, G.; Vantomme, G.; Dankers, P. Y. W.; Meijer, E. W. Supramolecular Polymers Form Tactoids through Liquid–Liquid Phase Separation. Nature 2024, 626 (8001), 1011–1018. https://doi.org/10.1038/s41586-024-07034-7.
(16) Kumar, M.; Hanssen, Job. N. S.; Dhiman, S. Unveiling the Liquid-Liquid Phase Separation of Benzene-1,3,5-Tricarboxamide in Water. ChemSystemsChem 2024, 6 (4). https://doi.org/10.1002/syst.202400013.
(17) Yewdall, N. A.; André, A. A. M.; Lu, T.; Spruijt, E. Coacervates as Models of Membraneless Organelles. Curr Opin Colloid Interface Sci 2021, 52, 101416. https://doi.org/10.1016/j.cocis.2020.101416.
(18) Wang, B.; Zhang, L.; Dai, T.; Qin, Z.; Lu, H.; Zhang, L.; Zhou, F. Liquid–Liquid Phase Separation in Human Health and Diseases. Signal Transduct Target Ther 2021, 6 (1), 290. https://doi.org/10.1038/s41392-021-00678-1.
(19) Tong, X.; Tang, R.; Xu, J.; Wang, W.; Zhao, Y.; Yu, X.; Shi, S. Liquid–Liquid Phase Separation in Tumor Biology. Signal Transduct Target Ther 2022, 7 (1), 221. https://doi.org/10.1038/s41392-022-01076-x.
(20) Zheng, L. W.; Liu, C. C.; Yu, K. Da. Phase Separations in Oncogenesis, Tumor Progressions and Metastasis: A Glance from Hallmarks of Cancer. Journal of Hematology and Oncology. BioMed Central Ltd December 1, 2023, p 123. https://doi.org/10.1186/s13045-023-01522-5.
(21) Boija, A.; Klein, I. A.; Young, R. A. Biomolecular Condensates and Cancer. Cancer Cell 2021, 39 (2), 174–192. https://doi.org/10.1016/j.ccell.2020.12.003.
(22) Li, Y. R.; King, O. D.; Shorter, J.; Gitler, A. D. Stress Granules as Crucibles of ALS Pathogenesis. Journal of Cell Biology 2013, 201 (3), 361–372. https://doi.org/10.1083/jcb.201302044.
(23) Molliex, A.; Temirov, J.; Lee, J.; Coughlin, M.; Kanagaraj, A. P.; Kim, H. J.; Mittag, T.; Taylor, J. P. Phase Separation by Low Complexity Domains Promotes Stress Granule Assembly and Drives Pathological Fibrillization. Cell 2015, 163 (1), 123–133. https://doi.org/10.1016/j.cell.2015.09.015.
(24) Mackenzie, I. R.; Nicholson, A. M.; Sarkar, M.; Messing, J.; Purice, M. D.; Pottier, C.; Annu, K.; Baker, M.; Perkerson, R. B.; Kurti, A.; Matchett, B. J.; Mittag, T.; Temirov, J.; Hsiung, G.-Y. R.; Krieger, C.; Murray, M. E.; Kato, M.; Fryer, J. D.; Petrucelli, L.; Zinman, L.; Weintraub, S.; Mesulam, M.; Keith, J.; Zivkovic, S. A.; Hirsch-Reinshagen, V.; Roos, R. P.; Züchner, S.; Graff-Radford, N. R.; Petersen, R. C.; Caselli, R. J.; Wszolek, Z. K.; Finger, E.; Lippa, C.; Lacomis, D.; Stewart, H.; Dickson, D. W.; Kim, H. J.; Rogaeva, E.; Bigio, E.; Boylan, K. B.; Taylor, J. P.; Rademakers, R. TIA1 Mutations in Amyotrophic Lateral Sclerosis and Frontotemporal Dementia Promote Phase Separation and Alter Stress Granule Dynamics. Neuron 2017, 95 (4), 808-816.e9. https://doi.org/10.1016/j.neuron.2017.07.025.
(25) Kanaan, N. M.; Hamel, C.; Grabinski, T.; Combs, B. Liquid-Liquid Phase Separation Induces Pathogenic Tau Conformations in Vitro. Nat Commun 2020, 11 (1), 2809. https://doi.org/10.1038/s41467-020-16580-3.
(26) Morelli, C.; Faltova, L.; Capasso Palmiero, U.; Makasewicz, K.; Papp, M.; Jacquat, R. P. B.; Pinotsi, D.; Arosio, P. RNA Modulates HnRNPA1A Amyloid Formation Mediated by Biomolecular Condensates. Nat Chem 2024, 16 (7), 1052–1061. https://doi.org/10.1038/s41557-024-01467-3.
(27) Darling, A. L.; Shorter, J. Combating Deleterious Phase Transitions in Neurodegenerative Disease. Biochimica et Biophysica Acta (BBA) - Molecular Cell Research 2021, 1868 (5), 118984. https://doi.org/10.1016/j.bbamcr.2021.118984.
(28) Vendruscolo, M.; Fuxreiter, M. Protein Condensation Diseases: Therapeutic Opportunities. Nat Commun 2022, 13 (1), 5550. https://doi.org/10.1038/s41467-022-32940-7.
(29) Leenders, C. M. A.; Albertazzi, L.; Mes, T.; Koenigs, M. M. E.; Palmans, A. R. A.; Meijer, E. W. Supramolecular Polymerization in Water Harnessing Both Hydrophobic Effects and Hydrogen Bond Formation. Chemical Communications 2013, 49 (19), 1963. https://doi.org/10.1039/c3cc38949a.
(30) Hendrikse, S. I. S.; Su, L.; Hogervorst, T. P.; Lafleur, R. P. M.; Lou, X.; van der Marel, G. A.; Codee, J. D. C.; Meijer, E. W. Elucidating the Ordering in Self-Assembled Glycocalyx Mimicking Supramolecular Copolymers in Water. J Am Chem Soc 2019, 141 (35), 13877–13886. https://doi.org/10.1021/jacs.9b06607.
(31) Vantomme, G.; ter Huurne, G. M.; Kulkarni, C.; ten Eikelder, H. M. M.; Markvoort, A. J.; Palmans, A. R. A.; Meijer, E. W. Tuning the Length of Cooperative Supramolecular Polymers under Thermodynamic Control. J Am Chem Soc 2019, 141 (45), 18278–18285. https://doi.org/10.1021/jacs.9b09443.
(32) Fuentes, E.; Gabaldón, Y.; Collado, M.; Dhiman, S.; Berrocal, J. A.; Pujals, S.; Albertazzi, L. Supramolecular Stability of Benzene-1,3,5-Tricarboxamide Supramolecular Polymers in Biological Media: Beyond the Stability-Responsiveness Trade-Off. J Am Chem Soc 2022, 144 (46), 21196–21205. https://doi.org/10.1021/jacs.2c08528.
(33) Rijns, L.; Duijs, H.; Lafleur, R. P. M.; Cardinaels, R.; Palmans, A. R. A.; Dankers, P. Y. W.; Su, L. Molecularly Engineered Supramolecular Thermoresponsive Hydrogels with Tunable Mechanical and Dynamic Properties. Biomacromolecules 2024. https://doi.org/10.1021/acs.biomac.3c01357.
(34) Fuentes, E.; Gerth, M.; Berrocal, J. A.; Matera, C.; Gorostiza, P.; Voets, I. K.; Pujals, S.; Albertazzi, L. An Azobenzene-Based Single-Component Supramolecular Polymer Responsive to Multiple Stimuli in Water. J Am Chem Soc 2020, 142 (22), 10069–10078. https://doi.org/10.1021/jacs.0c02067.
(35) Su, L.; Mosquera, J.; Mabesoone, M. F. J.; Schoenmakers, S. M. C.; Muller, C.; Vleugels, M. E. J.; Dhiman, S.; Wijker, S.; Palmans, A. R. A.; Meijer, E. W. Dilution-Induced Gel-Sol-Gel-Sol Transitions by Competitive Supramolecular Pathways in Water. Science (1979) 2022, 377 (6602), 213–218. https://doi.org/10.1126/science.abn3438.
(36) Albertazzi, L.; van der Zwaag, D.; Leenders, C. M. A.; Fitzner, R.; van der Hofstad, R. W.; Meijer, E. W. Probing Exchange Pathways in One-Dimensional Aggregates with Super-Resolution Microscopy. Science (1979) 2014, 344 (6183), 491–495. https://doi.org/10.1126/science.1250945.
(37) Qian, D.; Michaels, T. C. T.; Knowles, T. P. J. Analytical Solution to the Flory-Huggins Model. Journal of Physical Chemistry Letters 2022, 13 (33), 7853–7860. https://doi.org/10.1021/acs.jpclett.2c01986.
(38) Wang, F.; Altschuh, P.; Ratke, L.; Zhang, H.; Selzer, M.; Nestler, B. Progress Report on Phase Separation in Polymer

Solutions. Advanced Materials 2019, 31 (26). https://doi.org/10.1002/adma.201806733.
(39) Ruff, K. M.; Roberts, S.; Chilkoti, A.; Pappu, R. V. Advances in Understanding Stimulus-Responsive Phase Behavior of Intrinsically Disordered Protein Polymers. J Mol Biol 2018, 430 (23), 4619–4635. https://doi.org/10.1016/j.jmb.2018.06.031.
(40) Tsai, Y. R.; Lin, S. T. Prediction and Reasoning for the Occurrence of Lower Critical Solution Temperature in Aqueous Solution of Ionic Liquids. Ind Eng Chem Res 2019, 58 (23), 10064–10072. https://doi.org/10.1021/acs.iecr.9b02551.
(41) Azzari, P.; Mezzenga, R. LLPS vs. LLCPS: Analogies and Differences. Soft Matter 2023, 19 (10), 1873–1881. https://doi.org/10.1039/D2SM01455F.
(42) Tanaka, H. Viscoelastic Phase Separation in Biological Cells. Commun Phys 2022, 5 (1), 167. https://doi.org/10.1038/s42005-022-00947-7.
(43) Adelizzi, B.; Aloi, A.; Markvoort, A. J.; Ten Eikelder, H. M. M.; Voets, I. K.; Palmans, A. R. A.; Meijer, E. W. Supramolecular Block Copolymers under Thermodynamic Control. J Am Chem Soc 2018, 140 (23), 7168–7175. https://doi.org/10.1021/jacs.8b02706.
(44) Leenders, C. M. A.; Albertazzi, L.; Mes, T.; Koenigs, M. M. E.; Palmans, A. R. A.; Meijer, E. W. Supramolecular Polymerization in Water Harnessing Both Hydrophobic Effects and Hydrogen Bond Formation. Chemical Communications 2013, 49 (19), 1963. https://doi.org/10.1039/c3cc38949a.
(45) Klein, I. A.; Boija, A.; Afeyan, L. K.; Hawken, S. W.; Fan, M.; Dall'Agnese, A.; Oksuz, O.; Henninger, J. E.; Shrinivas, K.; Sabari, B. R.; Sagi, I.; Clark, V. E.; Platt, J. M.; Kar, M.; McCall, P. M.; Zamudio, A. V; Manteiga, J. C.; Coffey, E. L.; Li, C. H.; Hannett, N. M.; Guo, Y. E.; Decker, T.-M.; Lee, T. I.; Zhang, T.; Weng, J.-K.; Taatjes, D. J.; Chakraborty, A.; Sharp, P. A.; Chang, Y. T.; Hyman, A. A.; Gray, N. S.; Young, R. A. Partitioning of Cancer Therapeutics in Nuclear Condensates. Science (1979) 2020, 368 (6497), 1386–1392. https://doi.org/10.1126/science.aaz4427.
(46) Kilgore, H. R.; Young, R. A. Learning the Chemical Grammar of Biomolecular Condensates. Nat Chem Biol 2022, 18 (12), 1298–1306. https://doi.org/10.1038/s41589-022-01046-y.

Insert Table of Contents artwork here